Publications of the Astronomical Society of the Pacific, 137:024503 (21pp), 2025 February https://doi.org/10.1088/1538-3873/adb2c1

A Flexible Spherical Mixture Model for Gamma-Ray Burst Patterns Obtained from BATSE and FERMI Mission

Prithwish Ghosh[1], Sujit Ghosh[1], and Debashis Chatterjee[2]
[1] Department of Statistics, North Carolina State University, 5109, SAS Hall, 2311 Stinson Dr, Raleigh, NC 27607, USA
[2] Department of Statistics, Visva Bharati University, Siksha Bhavana (Institute of Science), Santiniketan, Bolpur, WB 731235, India
Received 2024 November 18; revised 2025 February 4; accepted 2025 February 5; published 2025 February 24

Abstract

The study encapsulates the investigation into the spherical distributional characteristics of parameters relevant to Gamma-Ray Bursts (GRBs), mainly focusing on their Galactic coordinates. The study utilized a mixture of von Mises Fisher spherical distributions to model the spatial distribution of GRBs in both BATSE and FERMI catalogs. Optimal numbers of mixture components were determined for different subsets of GRBs, including Long and Short GRBs. For the BATSE catalog, it turns out that a mixture of two spherical distributions provides a good fit for the whole data set and long and short GRBs. On the other hand, for the FERMI catalog, it turns out that a mixture of three spherical distributions provides a good fit for the whole data set, and a mixture of four distributions is adequate for both long and short GRBs. Additionally, an assessment was made to determine if the location parameter of GRBs follows any spherical distribution. Our flexible directional statistical modeling framework reveals that GRBs exhibit a non-uniform distribution on the celestial sphere, as evidenced by rejecting the null hypothesis of uniform distribution on a sphere using the Watson test. Our analysis statistically inquires the long-held assumption of their isotropic spread, especially in 2D projected spatial distributions of GRBs, suggesting that these cosmic events might not be uniformly scattered across the celestial sphere. The observed clumping of GRBs hints at the underlying cosmic scaffolding—the large-scale distribution of matter and star formation. Our results statistically asserts the explanation that the intrinsic GRB formation rate is typically tied to cosmic star formation rates with a delay time distribution, leading to a non-uniform rate as a function of redshift, demanding more nuanced calculations. However, this finding needs to consider potential biases introduced by the Milky Way's obscuration and our heliocentric perspective.

Unified Astronomy Thesaurus concepts: Gamma-ray bursters (1878); Astronomy data analysis (1858); Astrostatistics (1882); Astrostatistics distributions (1884)

1. Introduction

Gamma-ray bursts (GRBs), the most luminous explosions in the universe, have captivated scientists for decades due to their immense energy release, brief duration, and enigmatic origins (Hakkila et al. 2000a; Gehrels et al. 2005). GRBs, these celestial powerhouses marked by their brief yet luminous gamma-ray flashes, originate from the cataclysmic mergers of neutron stars or a neutron star–black hole dance (Fishman & Meegan 1995), culminating in the birth of a stellar mass black hole. However, a crucial aspect, the spatial distribution of these bursts, remains largely unexplored. The prevailing assumption has been that GRBs exhibit isotropy, meaning they are randomly and uniformly scattered across the celestial sphere (Piran 1992, 2005). This assumption has underpinned numerous analyses and theoretical frameworks. However, recent advancements in observational techniques and statistical methods have opened doors to revisiting this long-held belief.

Directional statistical methodologies (Mardia 1972; Jammalamadaka & SenGupta 2001) for GRB properties analysis can potentially revolutionize our understanding of GRBs (Mardia 1972). Unveiling directional anisotropies could hold profound implications for the cosmological environment surrounding GRB progenitors and the distribution of matter in the universe. Additionally, directional classifications could provide crucial insights into the physical mechanisms responsible for these enigmatic explosions (Chatterjee & Ghosh 2023, 2024).

Thorough examinations of afterglow emissions, providing crucial insights into GRBs' dynamic characteristics and environments, have been conducted (see Piran 2005 for a comprehensive review). Supernova light curves detected in the afterglows of long-duration GRBs nearby have suggested that some GRBs occur during the collapse of massive stars (see Woosley & Bloom 2006 for a comprehensive review). This

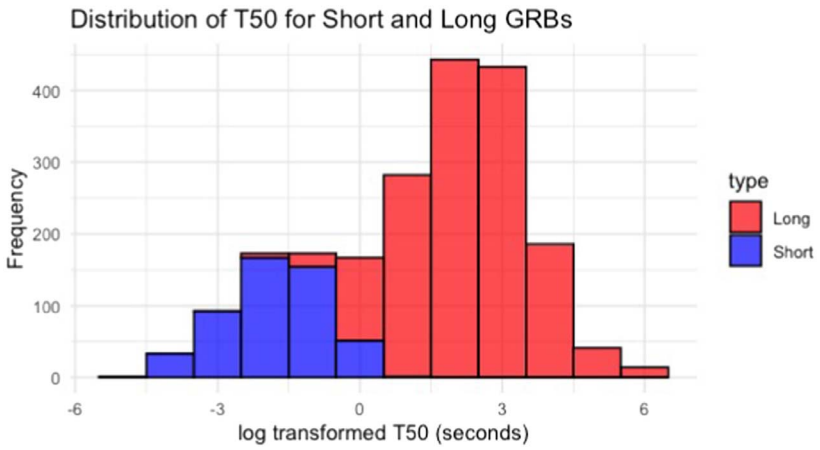

Figure 1. Bar Chart of the duration parameter t50 with respect to observed GRBs of BATSE Catalog.

classification is essential for identifying spectral or temporal correlations unique to GRB classes (Piran 1992; Gehrels et al. 2005; Bloom et al. 2006). In a general classification, GRBs have been categorized into two groups based on duration: long (>2 s) and short (<2 s) bursts This distinction arises from visually examining the burst duration distribution, revealing two distinct peaks Svinkin et al. (2019). Theoretically, long bursts may be associated with collapsing stars, where the event duration correlates with the dynamical collapse timescale. Conversely, the merger of two neutron stars will result in short-duration bursts (Ghosh & Chakraborty 2022). In this context, long-duration bursts should consistently be linked with supernova explosions in starburst regions. On the other hand, short bursts should exhibit no connection to starburst regions and lack associated supernovae (King et al. 2007).

Observationally, there are indications of more than two classes of GRBs, with some recorded instances displaying low intrinsic luminosity and deviating from standard spectral relationships (Sazonov et al. 2004; Soderberg et al. 2004). The absence of a supernova light curve in certain long-duration bursts, such as GRB 060614 and 060505, challenges the assumption that all such bursts arise from massive stellar collapse (Fynbo et al. 2006; Gehrels et al. 2006), although disputes exist, as in the case of GRB 060614 by Schaefer & Xiao (2006), who argue against its proximity. While awaiting confirmation of these findings, they underscore the possibility of more than two types of GRBs (Chattopadhyay et al. 2007). As mentioned above, we have shown the basic classification of GRBs with respect to their duration parameter in the figures below, where the red color is defined as a long GRB, and the blue color is defined as a short GRB. The Figures 1 and 2 are done for the BATSE Catalog, and the Figures 3 and 4 is done for the FERMI catalog. Recent observations, such as GRB 211211A (Rastinejad et al. 2022) and GRB 230307A (Levan et al. 2024), have identified kilonovae associated with long-duration GRBs, indicating that some long GRBs may originate from neutron star mergers rather than collapsing massive stars. These findings suggest that the duration-based classification may not perfectly correspond to distinct progenitor classes.

1.1. BATSE Catalog of Gamma-Ray Bursts

The Burst and Transient Source Experiment (BATSE; Preece et al. 2000) on the Compton Gamma-Ray Observatory (CGRO; Gehrels et al. 1993) has contributed spectral and temporal information for over 1900 GRBs. Despite the availability of several spectral parameters in the BATSE catalog, the bimodal distribution of GRBs is primarily based on univariate analysis, considering only duration as a parameter (e.g., Dezalay et al. 1992; Kouveliotou et al. 1993). Some argue that even this univariate analysis supports the existence of three classes (Horváth 1998). McLean et al. (2012) undertook initial multivariate analyses, followed by various classification approaches, such as neural network techniques (Baumgart 1994), factor analysis (Bagoly et al. 1998), nonparametric hierarchical clustering (Mukherjee et al. 1998; Balastegui et al. 2001), and unsupervised pattern recognition algorithms (Hakkila et al. 2003).

Figure 5 (Hammer-Aitoff projection) visualizes the distribution of BATSE GRBs across the sky. It is an overall BATSE GRB Aitoff plot all over the skymap using ALADIN software (Boch et al. 2011).

Critically, these analyses are subject to observational biases inherent in the observed properties of GRBs (Hakkila et al. 2000b). Hakkila et al. (2000a) argue that classification techniques are significantly hindered by these biases, possibly contributing to the identification of two classes (see Horváth et al. 2006 for a counterargument).

Spatial analysis based on the Galactic coordinates of GRBs in the BATSE catalog is relatively limited, with most studies

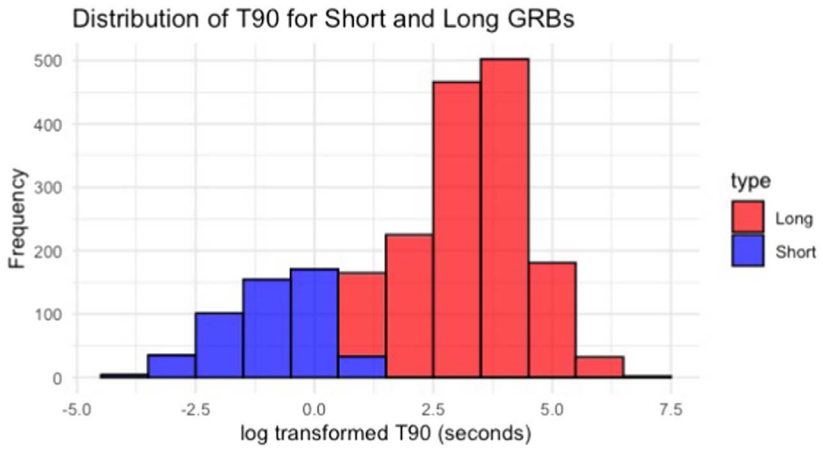

Figure 2. Bar Chart of the duration parameter t90 with respect to observed GRBs of BATSE Catalog.

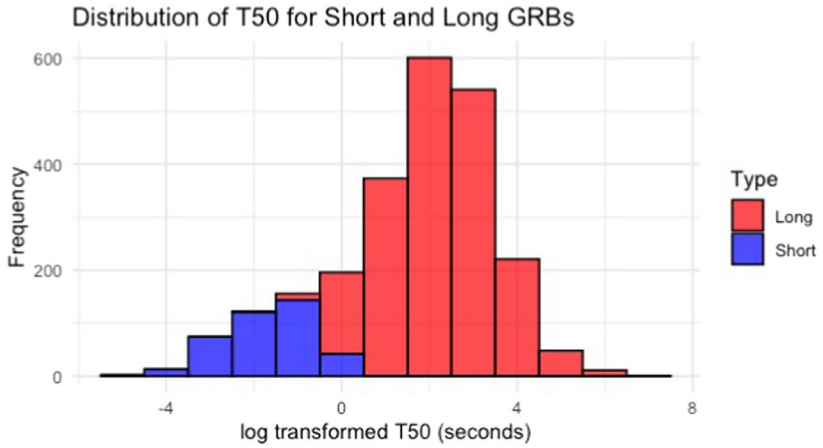

Figure 3. Bar Chart of the duration parameter t50 with respect to observed GRBs of FERMI Catalog.

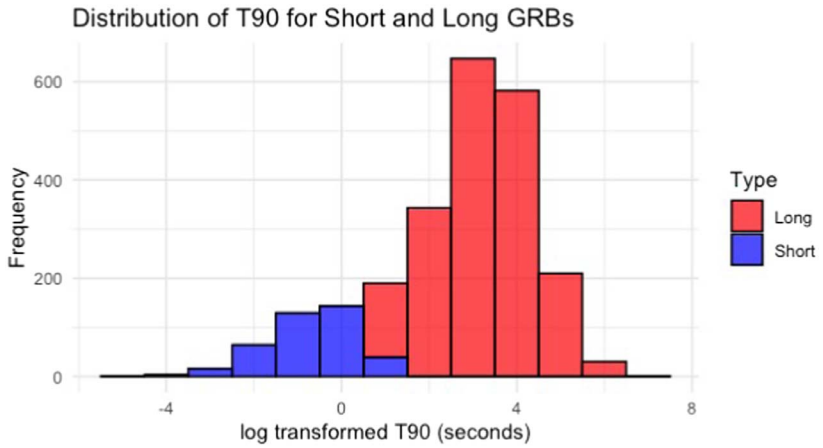

Figure 4. Bar Chart of the duration parameter t90 with respect to observed GRBs of FERMI Catalog.

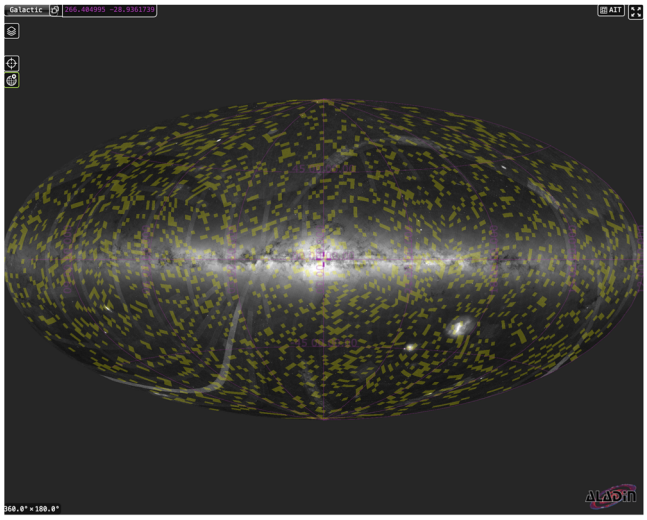

Figure 5. This Aitoff plot (Hammer-Aitoff projection) visualizes the distribution of BATSE Gamma-Ray Bursts (GRBs) across the sky. The data was processed using the ALADIN software.

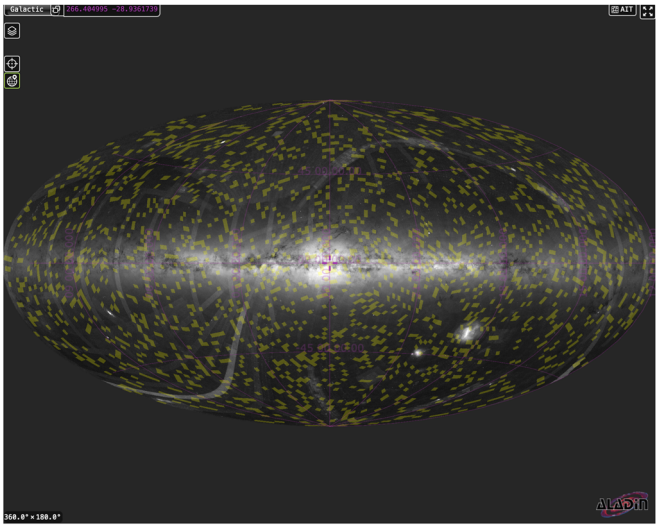

Figure 6. This Aitoff plot visualizes the distribution of FERMI Gamma-Ray Bursts (GRBs) across the sky. The data was processed using the ALADIN software.

focusing on linear analyses. However, literature is scarce exploring the spatial mixture model distributional fit in detail (Meegan et al. 1992; Hakkila et al. 1994). Existing research primarily delves into linear methods, leaving a gap in understanding the complex spatial distribution of GRBs within the Galactic coordinate system using Spherical or Circular Statistics (Anchordoqui et al. 2020; Goldstein et al. 2020). Therefore, further exploration and analysis using spatial mixture models could offer valuable insights into the spatial distribution patterns of GRBs in the BATSE catalog.

1.2. Fermi Catalog of Gamma-Ray Bursts

The Fermi-GBM science team regularly publishes catalogs summarizing the critical characteristics of triggered bursts, consolidating data from several completed mission years (Koshut et al. 1996; von Kienlin et al. 2014; Bhat et al. 2016). Accompanying the first two catalogs were spectral catalogs (Gruber et al. 2014; Connaughton et al. 2015) offering detailed spectral information on nearly all GRBs, including time-integrated fluence and peak flux spectra. Time-resolved spectral analysis for the brightest 81 GRBs from the first four mission years is available in the initial time-resolved spectral catalog (Yu et al. 2016), with ongoing work for a forthcoming catalog (Ajello et al. 2021, in preparation).

Various studies utilizing previous GBM catalogs have been documented elsewhere (e.g., Kovacevic et al. 2014; Calderone et al. 2015; Charisi et al. 2015; Kaneko et al. 2015; Tarnopolski 2015; Bhat et al. 2016; Abbott et al. 2017b; Andrade et al. 2019). Additionally, we underscore the significance of GBM data in multi-messenger astrophysics, particularly after the landmark detection of simultaneous gravitational waves (GWs) and electromagnetic (EM) radiation from the binary neutron star merger event on 2017 August 17 (Goldstein et al. 2012; Abbott et al. 2017a). Subsequently, an investigation of GBM data for GRBs resembling GRB 170817A was conducted over the entire duration of the current catalog (von Kienlin et al. 2012). Thirteen candidates were identified during ten mission years, suggesting that Fermi-GBM may trigger onboard approximately one burst akin to GRB 170817A per year.

In the Figure 6, an overall GRB plot concerning Aitoff plot and plotted all over the skymap using ALADIN software Boch et al. (2011).

The spatial analysis of the FERMI GRB catalog, particularly concerning Galactic coordinates, has been relatively limited compared to other aspects of GRB research. Existing studies often focus on linear analyses (Aasi et al. 2014; Goldstein et al. 2020), and there is a similar scarcity of literature addressing spatial mixture model distributional fits for circular distribution as BATSE catalog. This gap in research presents an opportunity to delve deeper into the spatial characteristics of FERMI GRBs using advanced statistical techniques such as mixture models. By exploring the spatial distribution of FERMI GRBs, researchers can uncover valuable insights into their spatial clustering, dispersion patterns, and underlying spatial processes, enhancing our understanding of these astrophysical phenomena (Akerlof & Swan 2007; Fleischer 2012).

1.3. Objectives and Novelty of this Paper

1. Considering the directional nature of Galactic coordinates, the study employs statistical methodologies suited

for directional data, explicitly investigating the circular distributions of the Galactic coordinatess of observed GRBs. Earlier, Duque & Marinucci (2023) discussed Geometric methods for cosmological data and highlighted recent advancements in spherical data analysis, mainly for cosmology, covering cosmological motivations, spectral representations, needlet/wavelet frames, map reconstruction, and tests for Gaussianity and isotropy.

2. Specifically, our study examines the directional probabilistic distributions of the Galactic coordinatess of observed GRBs and fits a spherical distribution of a von Mises–Fisher (vMF) mixture. Proposing a future predictive classification technique by giving a Spherical mixture distribution, where if we lack the observation of physical parameters of the Observed GRB data, we can use that for predictive classification of GRBs.
3. The analysis is performed on an imputed data set sourced from the BATSE and FERMI Catalogs, which complements each other regarding temporal coverage and detection capabilities, thereby enhancing the robustness and reliability of the findings.
4. This study innovatively applies a mixture of von Mises Fisher spherical distributions to model the spatial distribution of GRBs in the BATSE and FERMI catalogs, revealing non-uniform distributions. For the BATSE catalog, a mixture of two spherical distributions fits well, while the FERMI catalog requires a mixture of three or four distributions for different subsets of GRBs. Under certain limitations and assumptions discussed in Section 8.3, the analysis challenges the long-held assumption of isotropic GRB distribution, suggesting these cosmic events are not uniformly scattered across the celestial sphere. This clumping hints at an underlying cosmic structure, necessitating more nuanced astrophysical models and calculations.
5. Through this investigation, the paper contributes to a deeper understanding of GRB types and their characteristics, providing valuable insights into the statistical methods employed for their classification.

2. Data Set

The categorization of GRBs is based on two key parameters: T_{50} and T_{90} (Hakkila et al. 2000a). The BATSE aboard the CGRO supplied spectral and temporal details for over 1900 GRBs (Paciesas et al. 1999; Chattopadhyay et al. 2007). There are several parameters to classify the Classes of GRB (e.g., Mukherjee et al. 1998; Hakkila et al. 2000a). The sample comprises 1962 GRBs with nonzero detection of these parameters without introducing completeness criteria. We mainly used Galactic Longitude (GLON) and Galactic Latitude (GLAT) for a directional overview of the BATSE catalog and also used the FERMI GRB 4th catalog (Von Kienlin et al. 2020).

3. Methods

In analyzing GRBs, we employed directional statistical tools to investigate the spatial characteristics. Specifically, we used the Watson test to examine whether GRBs' observed GLON and GLAT follow a circular distribution. We introduced a von Mises Fishers mixture model to model the spatial components on a unit sphere.

3.1. Directional Statistical Distributions

We start with essential definitions and properties of some directional statistical distributions and directional statistical tests. For details, we refer to Jammalamadaka & SenGupta (2001), Kim & SenGupta (2018). Directional statistics, also known as circular statistics in 2D and spherical statistics in 3D, is the branch of statistics that deals with directions (angles), rotations, and orientations. These methods are particularly useful for analyzing data that is naturally constrained to lie on the surface of a sphere, such as geographical coordinates, wind directions, and orientations of molecules. Thus, the spatial distribution of GRBs observed over the celestial sphere could be analyzed using distributions supported on the surface of the sphere.

The vMF distribution (also known as the Fisher distribution) is used as a default choice in three dimensions. The vMF can be obtained as a restriction of any isotropic multivariate normal density to the unit hypersphere and thus this distribution plays a central role in directional statistics similar to a (multivariate) Gaussian distribution on the Euclidean space. It is defined on the unit sphere $S^2 = \{\boldsymbol{x} \in R^3 : ||\boldsymbol{x}|| = 1\}$ and is given by:

$$f_{\text{vMF}}(\boldsymbol{x}|\boldsymbol{\mu}, \kappa) = \frac{\kappa}{4\pi \sinh(\kappa)} \exp(\kappa \boldsymbol{\mu}^\top \boldsymbol{x}), \tag{1}$$

where x is a unit vector in R^3, $\boldsymbol{\mu} \in S^2$ is the mean direction vector, and $\kappa \geqslant 0$ is the concentration parameter. Notice that $\kappa = 0$ leads to a uniform distribution on the S^2. So, we are to assume that GRBs are distributed following a vMF distribution, then we would be testing the null hypothesis H_0: $\kappa = 0$ to test for uniformity of the GRBs.

3.2. Directional Mixture Model

A Spherical mixture model is used to see the spherical distributional pattern of how the observed GRBs are scattered around as per their Galactic coordinates if plotted over a Sky Map. The mixture model was previously proposed in Ghosh et al. (2024a), which is used here. We used the von Mises Fishers mixture distributional model as per the given Equation (2). This approach helps capture the multimodal nature of the data (Ghosh & Chatterjee 2023).

We define the density for a circular parametric mixture distributional model, which is denoted as $p(\boldsymbol{x}|\boldsymbol{\theta})$, as follows

$$p(\boldsymbol{x}|\boldsymbol{\theta}) = \sum_{j=1}^{K} \phi_j f_{\text{vMF}}(\boldsymbol{x}|\boldsymbol{\psi}_j), \tag{2}$$

where $\boldsymbol{\psi}_j = (\boldsymbol{\mu}_j, \kappa_j)$ as defined in Equation (1) and mixing weights $\phi_j \geqslant 0, \forall\, j$ satisfying the restriction $\sum_{j=1}^{K} \phi_j = 1$. The details of the parameter used in the above model are provided in our previous article Ghosh et al. (2024a). To empirically determine the optimal number of mixture components, we used Bayesian Information Criteria (BIC) instead of AIC, based on recommendations given in the article Zhang et al. (2023), which provides a comprehensive analysis to justify the use of BIC for mixture models used in our application. As per the article Zhang et al. (2023) BIC formula is given in the Equation (3):

$$\text{BIC}_m \stackrel{\Delta}{=} -2\sum_{i=1}^{n} \log p(x_i|\hat{\theta}_m) + d_m \log n, \tag{3}$$

where $p(x_i|\theta)$ is as defined in Equation (2) and d_m denotes the dimension of the mixture model. In addition to BIC used in the article Ghosh et al. (2024a), we used another criterion called Bridge Criteria (BC) to determine the optimal number of mixture components. We used the formula to calculate the Bridge Factor given in the articles Zhang et al. (2023) and Ding et al. (2017). Below, we provide further details of the BC (4).

$$\text{BC}_m \stackrel{\Delta}{=} -2\sum_{i=1}^{n} \log p(x_i|\hat{\theta}_m) + n^{2/3}\sum_{k=1}^{d_m} \frac{1}{k}. \tag{4}$$

In the mixture model case, if each component distribution has three parameters (e.g., two locations and a scale) and there are k components with weights adding to 1, then $d_m = 3k + k - 1 = 4k - 1$. The "two locations" represent two central tendency measures or positions in the data. The "scale" parameter describes the spread or dispersion of the data within each component. Each component distribution in the mixture is parameterized by a mean direction vector $\boldsymbol{\mu}_j \in S^2$ (described by two angular coordinates on the unit sphere) and a concentration parameter κ_j, which dictates the spread around the mean direction.

As per the above Equations (4) and (3) we can find the BC as per Equation (5)

$$\text{BC} = \text{BIC} + p_{\text{diff}} \tag{5}$$

where, $p_{\text{diff}} = n^{(2/3)} \sum_{k=1}^{d_m} \frac{1}{k} - d_m \log(n)$

We also cross-check with the AIC values as per the Equation (6)

$$\text{AIC}_m \stackrel{\Delta}{=} -2\sum_{i=1}^{n} \log p_{\hat{\theta}_m}(x_i) + 2d_m. \tag{6}$$

García-Portugués (2013) details how the optimized version of the mixture is calculated and plotted in the density plots, which we applied here (see Figure 8).

3.3. Identifiability and Estimation of Mixture Models

The paper Ho & Nguyen (2016) tackles key challenges in finite mixture models, specifically focusing on identifiability and estimation issues. The exchangeability of mixture components can cause different parameterizations of the same model to produce equivalent likelihoods, resulting in identifiability problems. This makes it difficult to uniquely identify the parameters of the mixture model. Additionally, selecting the appropriate number of mixture components (model selection) is often challenging, particularly when dealing with complex or noisy data. Optimization algorithms may converge to local rather than global maxima of the likelihood function, affecting parameter estimates' accuracy. Understanding the rate at which estimation algorithms converge to true parameter values is crucial for evaluating their efficiency and reliability. Ho & Nguyen (2016) explores the convergence rates of parameter estimation algorithms for finite mixture models, shedding light on how quickly these algorithms reach the true parameter values as the sample size grows. This understanding is essential for assessing estimation methods' computational complexity and effectiveness. In our application, we establish the strong identifiability using the Theorem 3.3 (d) of Ho & Nguyen (2016) for the univariate case. For the multivariate case, Chen (1995), has shown that the optimal convergence rate is $n^{-1/4}$ for a finite mixture model where the number of components is known within a certain upper limit. Specifically, Section 3 of Chen (1995) provides evidence that this convergence rate of $n^{-1/4}$ is attainable.

4. Results for the BATSE Catalog

In this study, we employed a vMF mixture model to provide a comprehensive overview of the spatial distribution of GRBs cataloged by the BATSE. Our analysis focused on understanding how these GRBs are distributed across the celestial sphere in terms of GLON and GLAT.

In Figure 7, we present a skymap depicting the distribution of long and short GRBs. Red dots denote long bursts, while blue dots represent short bursts, classified based on duration.

In this study, we analyzed the BATSE catalog data set by dividing it into three sections: the entire BATSE catalog (Section 4.1), short gamma bursts (Section 4.3), and long GRBs (Section 4.2).

4.1. Results for Directional and Spherical Statistical Analysis for Overall Gamma-Ray Bursts (BATSE Catalog)

Watson test results are given in the Table A1, where we used both 0.01 significance levels. We tested if the directional parameters (GLON, GLAT) GRB observed data points and checked whether they follow any circular distributions.

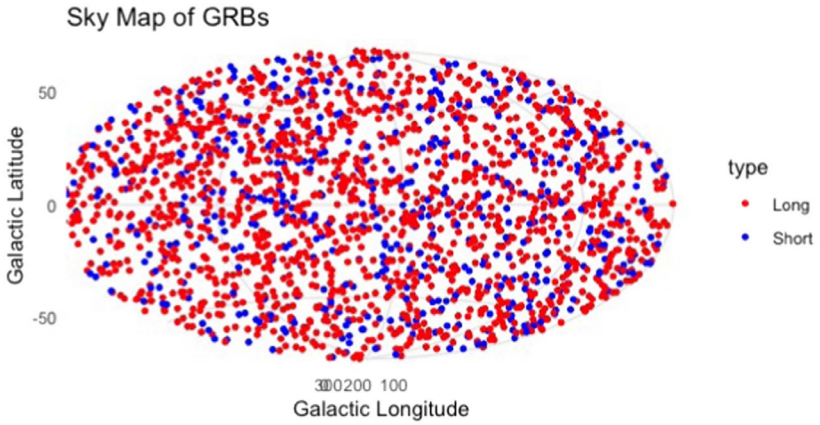

Figure 7. All-sky distribution of Long and Short Gamma-Ray Bursts (GRBs) from the BATSE catalog plotted on a celestial sky map. GRBs are classified as long (duration > 2 s)(Red dots) or short (duration $\leqslant 2$ s) (Blue). This plot visually represents the spatial distribution of these energetic events across the sky.

According to the results above, all the location parameters of GRB follow von Mises distribution and circular distributions.

We applied the vMF mixture model to gain insights into the spatial distribution of observed GRBs within the galactic sphere. Table 1 presents the BIC scores corresponding to different values of k. Combining the vMF distribution for the location parameters (GLON and GLAT), we assessed the model's performance across ten partitions, ranging from 1 to 10. Our analysis revealed that this data set's optimal number of partitions is 2. Similarly, we used AIC values, which gives us that the optimal number of partitions or Mixture is 6 (Given in the Table A7), and used BC, which gives us the optimal number of mixtures, which is 3 (Given in the Table 2).

The density plot of the BATSE GRB data set, generated using the Von Mises Fisher algorithm, is depicted in Figure 8, Figure 9. Within this visualization, observed GRB data points are denoted by black dots, while the contours representing the Von Mises Fisher distribution are illustrated in blue. Furthermore, the density plot of the data set itself is described in green. This comprehensive depiction provides a visual understanding of the spatial distribution of GRBs within the galactic sphere, as inferred through the application of the vMF algorithm.

Figure 8: Density plot of the BATSE GRB data set using the Von Mises Fisher algorithm. Black dots represent observed GRB data points, blue indicates the Von Mises Fisher contours, and green signifies the density plot of the data set.

4.2. Long Gamma-Ray Bursts Result

The Table A2 presents the outcomes of the Watson test, conducted with a significance level of 0.01. We aimed to assess whether the directional parameters (GLON, GLAT) associated with observed Long GRBs conform to any circular distributions. As per the findings, all location parameters of Long GRBs adhere to the von Mises distribution and exhibit circular behavior.

Table 1
Bayesian Information Criteria (BIC) Values for the Number of Mixture Components $k = 1, 2, \ldots$. From that, 2 Partitions can Combine Fisher Von Mises Distribution for the Location Parameter (GLON and GLAT)

Partition Number	BIC Values	Partition Number	BIC values
1	−5365.844	6	−5872.662
2	**−5901.839**	7	−5852.070
3	−5896.046	8	−5829.388
4	−5885.700	9	−5798.479
5	−5871.479	10	−5783.355

Note. We checked ten values of k from 1 to 10, where the optimal number of partitions is 2.

Table 2
Bridge Criteria Values for Number of Mixture Components $k = 1, 2, \ldots$. From that, 3 Partitions can Combine Fisher Von Mises Distribution for the Location Parameter (GLON and GLAT)

Partition Number	BC Values	Partition Number	BC values
1	−2406.17	6	−11169.48
2	−11331.49	7	−10740.05
3	**−14364.76**	8	−12733.48
4	−11181.91	9	−10779.30
5	−8712.61	10	−10668.20

Note. We checked ten values of k from 1 to 10, where the optimal number of partitions is 3.

Table 3 presents the BIC scores corresponding to each value of k. Utilizing this information, we determined that 2 partitions

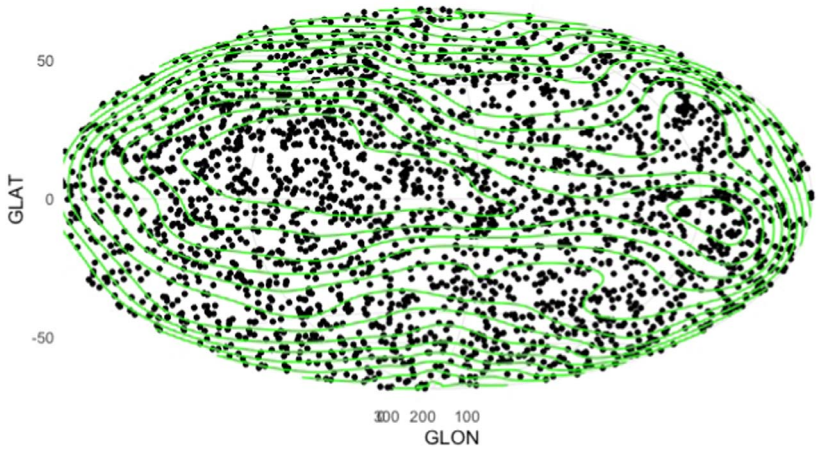

Figure 8. Density plot of the GRB data set where we used von Mises Fishers distribution. The black dots are observed GRB data points, the Green color indicates the density plot of the data set.

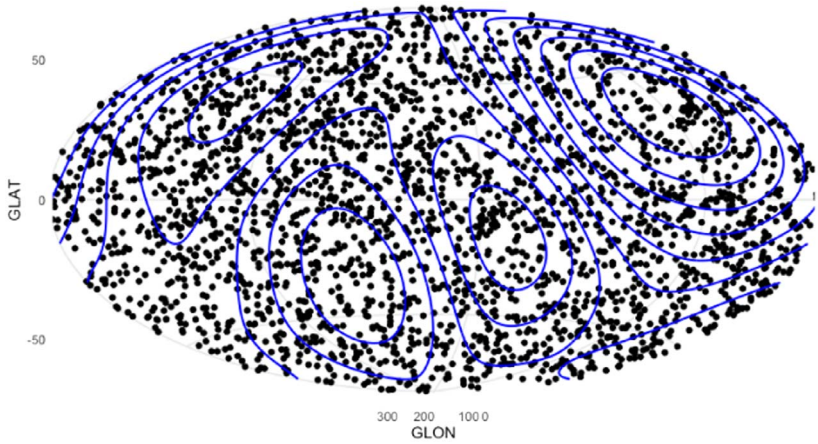

Figure 9. Density plot of the GRB data set where we used Von Mises Fishers distribution. The black dots are observed GRB data points, the Blue color indicates the Von Mises Fishers Contour of the data set.

can effectively integrate the Fisher von Mises Distribution for Long GRBs' location parameters (GLON and GLAT). Our analysis spanned ten values of k, ranging from 1 to 10, revealing that the optimal number of partitions for this data set is 2. Similarly, we used AIC values, which indicate that the optimal number of partitions or mixtures is 6 (as shown in Table A8). We also used the Bridge Criterion, which suggests that the optimal number of mixtures is 3 (as shown in Table 4). There is a total of 1345 samples under long GRBs.

The density plot in the Figure 10, Figure 11 depicts the distribution of the Long BATSE GRB data set, employing the Von Mises Fisher algorithm. The black dots represent the observed Long BATSE GRB data points, while the blue contours signify the representation of the vMF model. Additionally, the green shading illustrates the density plot derived from the data set, providing further insights into the spatial distribution of the observed Long BATSE GRBs.

Table 3
Table Containing the Bayesian Information Criteria Score for Each K Value

Partition Number	BIC Values	Partition Number	BIC Values
1	−4084.249	6	−4389.232
2	**−4443.7609**	7	−4367.182
3	−4435.524	8	−4347.116
4	−4421.244	9	−4325.418
5	−4406.229	10	−4319.634

Note. From that, two partitions can combine Fisher Von Mises Distribution for Long Gamma-Ray Bursts' location parameters (GLON and GLAT). We checked ten values of k from 1 to 10, where the optimal number of partitions is 2.

4.3. Short Gamma-Ray Bursts Result

From the Table A3, the results of the Watson test are provided herein, employing significance levels of 0.01. We

Table 4
Table Containing the Bridge Criteria for Each K Value

Partition Number	BC Values	Partition Number	BC Values
1	−2413.21	6	−11573.88
2	−10794.88	7	−10866.98
3	−9182.9	8	−9187.85
4	**−11584.73**	9	−11563.57
5	−11124.03	10	−8707.86

Note. From that, 4 partitions can combine Fisher von Mises Distribution for Long Gamma-Ray Bursts' location parameters (GLON and GLAT). We checked ten values of k from 1 to 10, where the optimal number of partitions is 4.

aimed to assess whether the directional parameters (GLON, GLAT) of observed data points for Short GRBs conform to any circular distributions. As per the findings, all location parameters associated with Short GRBs adhere to the von Mises distribution and exhibit circular characteristics.

The Table 5 displays the BIC scores for each value of k. Based on this analysis, we determined that the Fisher Von Mises Distribution for Long GRBs' location parameters (GLON and GLAT) can be effectively combined into 2 partitions. We explored ten different values of k, ranging from 1 to 10, and identified that the optimal number of partitions for this data set is 2. We also employed AIC values, which suggest that the optimal number of partitions or mixtures is 2 (refer to Table A9). In addition, we utilized the Bridge Criterion, which indicates that the optimal number of mixtures is 4 (refer to Table 6). There is a total of 694 samples under short GRBs.

The density plot in Figure 12, Figure 13 illustrates the Short BATSE GRB data set distribution using the Von Mises Fisher algorithm. The black dots represent the observed Short BATSE GRB data points, while the blue contour depicts the Von Mises Fisher distribution. Additionally, the green color indicates the density plot of the data set, offering a comprehensive visualization of the spatial distribution of the observed GRBs.

5. Results for the FERMI-GRB Catalog

Similarly, we utilized a vMF mixture model to comprehensively depict the spatial arrangement of GRBs documented by FERMI. Our investigation aimed to discern the distribution patterns of these GRBs across the celestial sphere, specifically concerning GLON and GLAT.

Figure 14 illustrates a skymap portraying the dispersion of both long and short GRBs. Red dots indicate long bursts, while short bursts are depicted by blue dots, categorized according to their duration.

We analyzed the BATSE catalog data set, partitioning it into three distinct sections: the complete BATSE catalog (refer to Section 5.1), short gamma bursts (refer to Section 5.3), and long GRBs (refer to Section 5.2).

5.1. Results for Directional and Spherical Statistical Analysis for Overall Gamma-ray Bursts (FERMI Catalog)

In the Table A4, here are the results of the Watson test, conducted with significance levels of 0.01. We aimed to ascertain whether observed Fermi GRBs' directional parameters (GLON, GLAT) adhere to circular distributions. Based on the outcomes, it is evident that all location parameters of Fermi GRBs conform to the von Mises distribution and circular distributions.

We generated a density plot for the Fermi GRB data set in the Figure 15, Figure 16 employing the vMF distribution. Within the plot, observed GRB data points are represented by black dots. The contours delineated in blue represent the Von Mises Fishers distribution, while the density plot of the data set is depicted in green.

The Table 7 presents the BIC scores corresponding to each value of K. These scores indicate the goodness of fit for different partitioning schemes. Our analysis suggests that three partitions can be combined using the Fisher von Mises distribution to model the spatial distribution of Fermi GRBs, considering the location parameters GLON and GLAT. We explored ten values of K ranging from 1 to 10, ultimately determining that the optimal number of partitions for this data set is 3. We also used AIC values, which indicate that the optimal number of partitions or mixtures is 5 (see Table A10). Additionally, we applied the Bridge Criterion, which suggests that the optimal number of mixtures is 5 (see Table 8).

5.2. Long FERMI Gamma-Ray Burst Result

As per the data set we have 1964 data points under the Long Fermi GRB which are captured. The Table A5 provides the following Watson test outcomes, employing significance levels of 0.01. Our objective was to examine the directional parameters (GLON, GLAT) concerning the observed data points of Long Fermi GRBs, aiming to ascertain their adherence to any circular distributions. Based on the findings indicated above, it is evident that all location parameters associated with Long Fermi GRBs conform to the von Mises distribution and circular distributions.

The density plot in the Figures 17 and 18 illustrates the Long Fermi GRB data set analyzed using the Von Mises Fishers Distribution. Each black dot represents an observed data point from the Long Fermi GRB data set. The blue contour delineates the Von Mises Fishers distribution, while the green overlay depicts the density plot of the data set.

The Table 9 showcases the BIC scores corresponding to various values of k. These scores serve as a metric for evaluating the goodness of fit for the Fisher von Mises

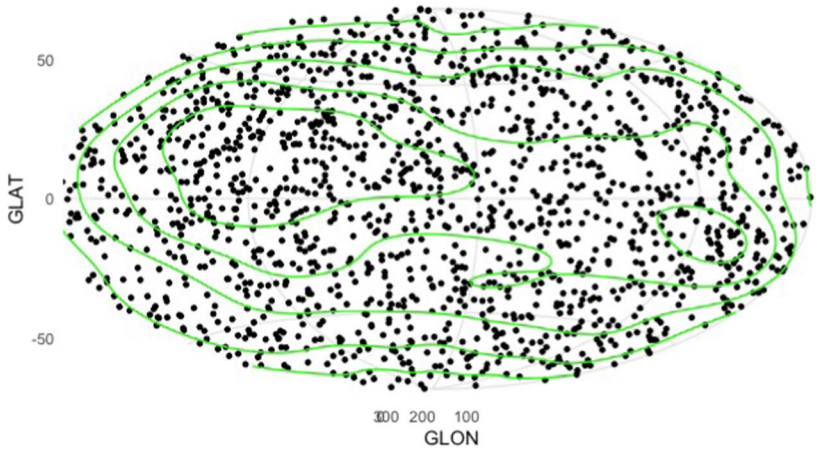

Figure 10. Density plot of the Long Batse GRB data set where we used Von Mises–Fisher distribution. The black dots are observed in Long BATSE GRB data points, the Green color indicates the density plot of the data set.

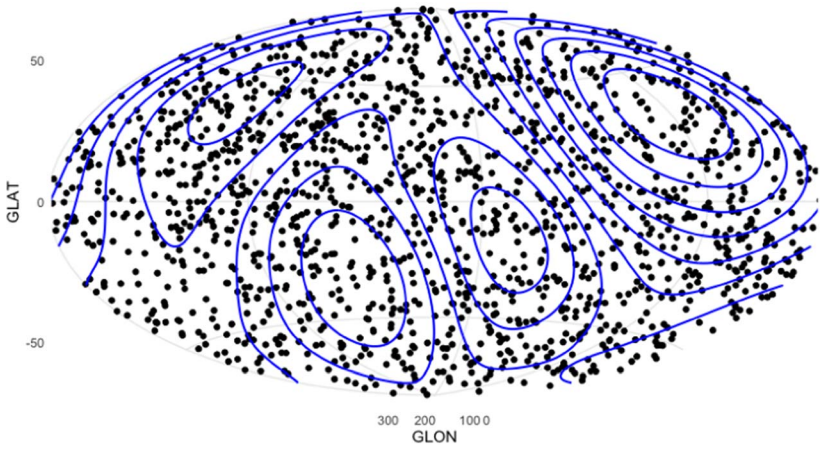

Figure 11. Density plot of the Long Batse GRB data set where we used Von Mises–Fisher distribution. The black dots are observed in Long BATSE GRB data points; the Blue color indicates the von Mises Fishers density plot of the data set.

Table 5
This Table Contains the Bayesian Information Criteria Score for Each K Value

Partition Number	BIC Values	Partition Number	BIC Values
1	−1272.111	6	−1390.289
2	**−1433.087**	7	−1371.877
3	−1427.712	8	−1354.066
4	−1408.395	9	−1335.499
5	−1402.708	10	−1320.035

Note. From that, 2 partitions can combine Fisher Von Mises Distribution for Long Gamma-Ray Bursts' location parameters (GLON and GLAT). We checked ten values of k from 1 to 10, where the optimal number of partitions is 2.

Table 6
This Table Contains the Bridge Criteria for Each K Value

Partition Number	BC Values	Partition Number	BC Values
1	−2393.50	6	−17983.17
2	−12444.73	7	−19577.71
3	−10341.60	8	−17674.75
4	**−22747.66**	9	−18148.35
5	−21246.60	10	−20341.25

Note. From that, 4 partitions can combine Fisher Von Mises Distribution for Long Gamma-Ray Bursts' location parameters (GLON and GLAT). We checked ten values of k from 1 to 10, where the optimal number of partitions is 4.

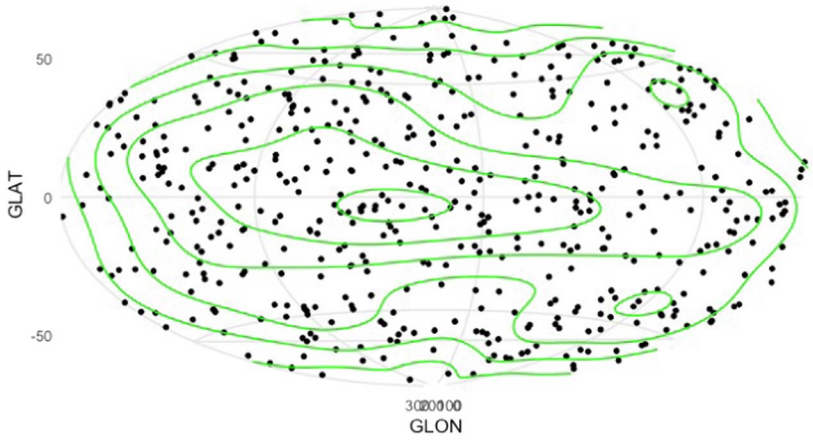

Figure 12. Density plot of the Short Batse GRB data set where we used Von Mises–Fisher distribution. The black dots are observed in Short BATSE GRB data points; the Green color indicates the density plot of the data set.

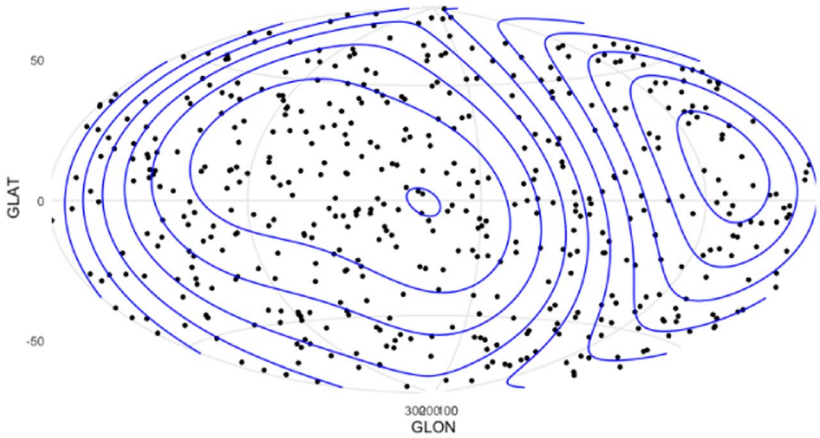

Figure 13. Density plot of the Short Batse GRB data set where we used Von Mises–Fisher distribution. The black dots are observed in Short BATSE GRB data points; the Blue color indicates the Von Mises Fishers Contour of the data set.

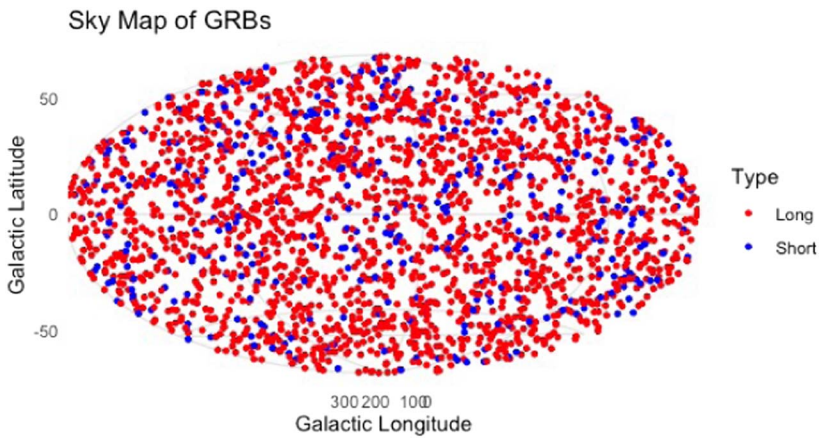

Figure 14. All-sky distribution of Long and Short Gamma-Ray Bursts (GRBs) from the FERMI catalog plotted on a celestial sky map. GRBs are classified as long (duration $>$ 2 s)(Red dots) or short (duration $\leqslant$ 2 s)(Blue). This plot provides a visual representation of the spatial distribution of these energetic events across the sky.

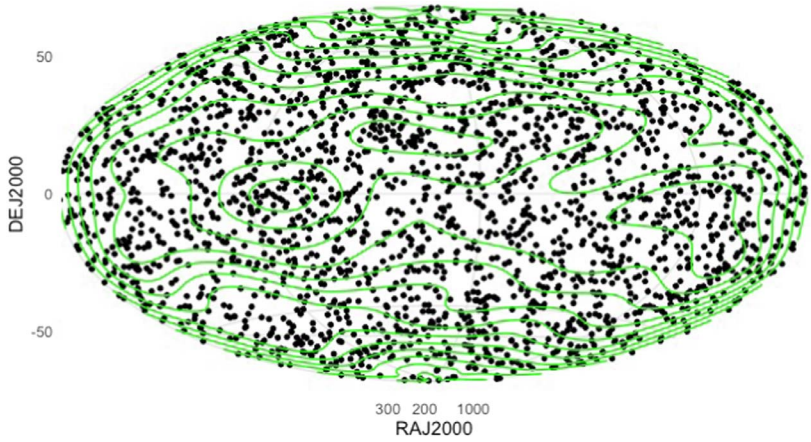

Figure 15. Density plot of the Fermi GRB data set where we used Von Mises–Fisher distribution. The black dots are observed GRB data points, the Green color indicates the density plot of the data set. This plot is done with respect to general density.

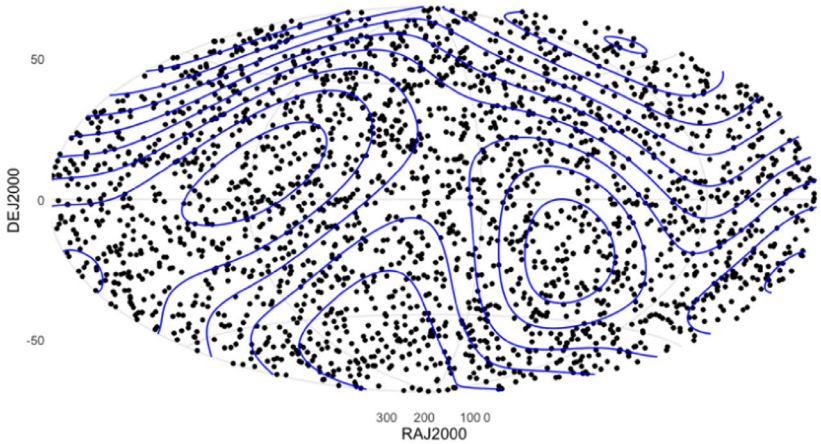

Figure 16. Density plot of the Fermi GRB data set where we used Von Mises–Fisher distribution. The black dots are observed GRB data points, the Blue color indicates the Von Mises Fishers Contour of the data set. This plot is done with respect to von Mises Fishers contour.

Table 7
Table Containing the Bayesian Information Criteria Score for Each K Value

Partition Number	BIC Values	Partition Number	BIC Values
1	−5870.361	6	−6444.040
2	−6469.389	7	−6430.734
3	**−6494.556**	8	−6414.509
4	−6485.317	9	−6382.862
5	−6465.160	10	−6366.028

Note. From that, 3 partitions can combine Fisher Von Mises Distribution for the location parameter(GLON and GLAT) of Fermi Gamma-ray Bursts. We checked ten values of k from 1 to 10, where the optimal number of partitions is 3.

Table 8
Table Containing the Bridge Criteria for Each K Value

Partition Number	BC Values	Partition Number	BC Values
1	−2064.34	6	−9825.81
2	−10532.28	7	−11553.01
3	−7858.22	8	−9112.97
4	−10777.97	9	−8525.6
5	**−11804.06**	10	−11381.78

Note. From that, Five partitions can combine Fisher Von Mises Distribution for the location parameter (GLON and GLAT) of Fermi Gamma-Ray Bursts. We checked ten values of k from 1 to 10, where the optimal number of partitions is 5.

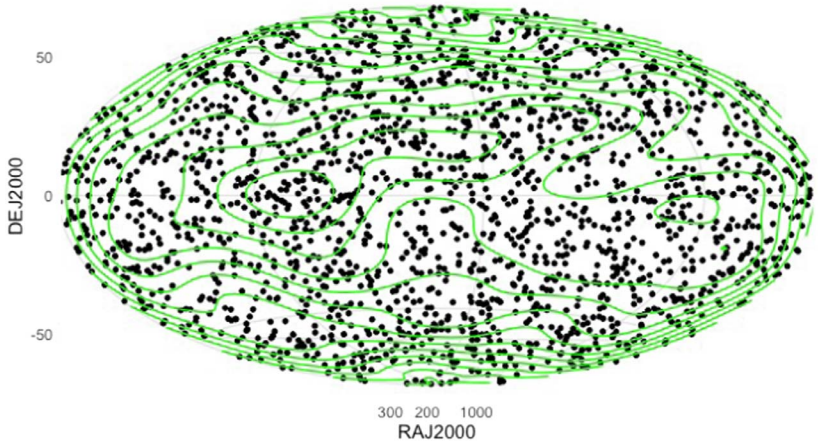

Figure 17. Density plot of the Long Fermi GRB data set where we used Von Mises–Fisher distribution. The black dots are observed in Long Fermi GRB data points; the Green color indicates the density plot of the data set. This is done with respect to the Density.

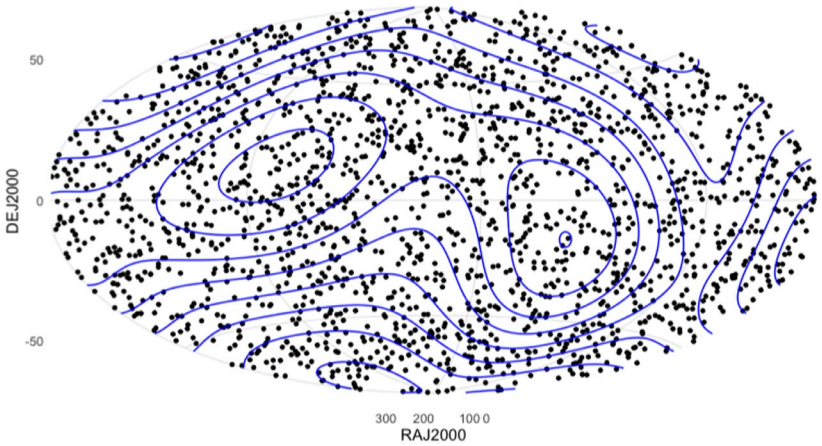

Figure 18. Density plot of the Long Fermi GRB data set where we used Von Mises–Fisher distribution. The black dots are observed in Long Fermi GRB data points; the Blue color indicates the Von Mises Fishers Contour, of the data set. This is done with respect to the von Mises Fishers contour plot.

distribution across Long Fermi GRBs' longitudinal (GLON) and latitudinal (GLAT) parameters. In our analysis, we explored ten different values of k, ranging from 1 to 10. Our findings suggest that this data set's most optimal partitioning strategy involves 4 distinct partitions. We also utilized the AIC values, which suggest that the optimal number of partitions or mixtures is 4 (refer to Table A11). Furthermore, we applied the Bridge Criterion, which indicates that the optimal number of mixtures is 5 (refer to Table 10).

5.3. Short FERMI Gamma-Ray Bursts

Results of the Watson test, mentioned in the Table A6 which is shown in the Appendix below, which is conducted at a significance level of 0.01. We aimed to ascertain whether the directional parameters (GLON and GLAT) associated with the observed data points of Short Fermi GRBs conform to any circular distributions. As per the findings, all Short Fermi GRBs' location parameters adhere to the von Mises distribution and circular distributions. The number of data points is 395.

Table 9
Table Containing the Bayesian Information Criteria Score for Each K Value

Partition Number	BIC Values	Partition Number	BIC Values
1	−4916.413	6	−5393.385
2	−5406.043	7	−5352.440
3	−5417.058	8	−5334.110
4	**−5400.920**	9	−5327.530
5	−5386.187	10	−5303.575

Note. From that, 4 partitions can combine Fisher Von Mises Distribution for Long Fermi Gamma-Ray Bursts' location parameters (GLON and GLAT). We checked ten values of k from 1 to 10, where the optimal number of partitions is 4.

The density plot in the Figure 19, Figure 20 depicts the Short Fermi GRB data set analyzed using the vMF distribution. In the

Table 10
Table Containing the Bridge Criteria Score for Each K Value

Partition Number	BC Values	Partition Number	BC Values
1	−2343.80	6	−11147.97
2	−11777.83	7	−10357.14
3	−9117.90	8	−6317.40
4	−9666.85	9	−7610.20
5	**−12745.18**	10	−5919.18

Note. From that, 5 partitions can combine Fisher Von Mises Distribution for Long Fermi Gamma-Ray Bursts' location parameters (GLON and GLAT). We checked ten values of k from 1 to 10, where the optimal number of partitions is 5.

plot, the observed Short Fermi GRB data points are represented by black dots. The blue color denotes the presence of the Von Mises Fishers Contour, while the green color illustrates the density plot of the data set.

The Table 11 provides the BIC scores corresponding to each value of k. Utilizing this data, we identified that the Fisher Von Mises Distribution for Short Fermi GRBs' location parameters (GLON and GLAT) can be effectively amalgamated into 4 partitions. By exploring ten different values of k ranging from 1 to 10, we determined that the optimal number of partitions for this analysis is 4. In addition, we employed the AIC values, which suggest that the optimal number of partitions or mixtures is 4 (see Table A12). Moreover, the application of the Bridge Criterion indicates that the optimal number of mixtures is 5 (see Table 12).

6. Discussion

6.1. Beyond Isotropy or Not?

Significance of Our Finding of Apparent Non-Isotropic Distribution of GRBs. Our directional statistical analysis provides compelling evidence that GRBs exhibit a non-isotropic distribution across the celestial sphere. This finding decisively contradicts a scenario where GRBs are uniformly distributed across the sky.

The critical result supporting this conclusion lies in rejecting the null hypothesis by the Watson test for both the BATSE and Fermi catalogs. Additionally, the optimal number of clusters identified by the BIC favoring a two-component vMF mixture model further strengthens the case for a non-uniform distribution.

This observed non-isotropy holds significant implications for our understanding of GRBs and the large-scale structure of the Universe:

1. *Tracer of Large-Scale Structure.* The non-uniform distribution of GRBs suggests that their progenitors, likely massive star cores or mergers of compact objects, are not randomly scattered throughout the cosmos. Instead, their clustering might reflect the underlying large-scale structure of the Universe, with higher concentrations in regions of enhanced star formation or specific galaxy types.
2. *Implications for GRB Rate Estimates.* A uniform distribution is often assumed for calculating the GRB rate within a given volume of space. Our findings indicate that this assumption might not be valid. By incorporating a more realistic, non-isotropic distribution model, astronomers can potentially refine estimates of the actual GRB rate and gain a more accurate picture of their occurrence across cosmic time.
3. *Progenitor Environments.* The identified sub-clusters within the GRB population using the two-component mixture model might point towards distinct progenitor environments. Future investigations can explore potential correlations between these clusters and other properties of GRBs, such as their redshift or host galaxies. This could provide valuable clues about the specific stellar or binary system configurations that lead to GRB formation.

6.2. Considering Observational Biases

Our directional statistical analysis suggests a non-isotropic distribution of GRBs in the celestial sphere. This finding challenges a uniform distribution, but it is crucial to acknowledge potential limitations in our observations.

While the Watson test rejection and the two-component vMF mixture model favor non-uniformity, we must consider the influence of:

1. *Milky Way Obscuration.* Our Galaxy, the Milky Way, contains significant dust and gas that can obscure GRBs, particularly at lower Galactic latitudes (GLAT). This obscuration bias could potentially affect the observed distribution, leading to an underrepresentation of GRBs in certain sky regions.
2. *Heliocentric Selection.* We observe the Universe from our position within the Milky Way. This heliocentric perspective might introduce a bias towards GRBs closer to the plane of our Galaxy. This could lead to an artificial clustering of GRBs along the Galactic plane, potentially mimicking a non-uniform distribution.

Mitigating these biases is essential for a definitive conclusion on the true isotropy of GRBs.

However, the observed non-isotropy, even considering these limitations, holds potential significance:

1. *Partial Evidence for Large-Scale Structure.* Despite potential observational biases, the non-uniform distribution might still offer a glimpse of the underlying large-scale structure of the Universe. Even if not the complete

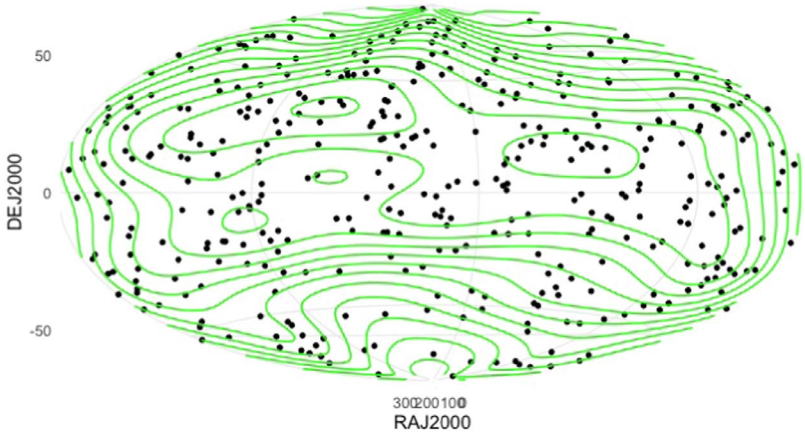

Figure 19. Density plot of the Short Fermi GRB data set where we used Von Mises–Fisher distribution. The black dots are observed in Short Fermi GRB data points, the Green color indicates the density plot of the data set. Density plot for the Fermi short gamma-ray burst.

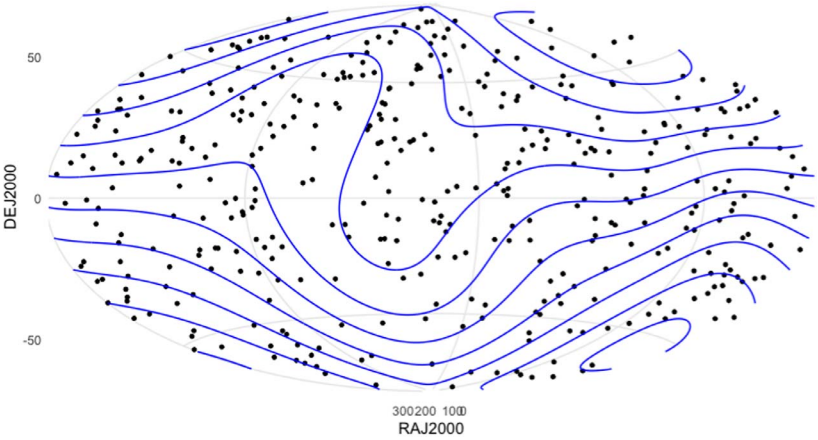

Figure 20. Density plot of the Short Fermi GRB data set where we used Von Mises–Fisher distribution. The black dots are observed in Short Fermi GRB data points, the Blue color indicates the Von Mises Fishers Contour of the data set. von Mises Fishers contour plot for the Fermi short gamma-ray burst.

picture, the clustering could reflect a real, albeit incomplete, distribution of GRB progenitors.

2. *Refined Rate Estimates and Future Missions.* Accounting for the non-isotropy and future efforts to correct obscuration and heliocentric biases can lead to more refined estimates of the actual GRB rate. Additionally, missions designed to observe GRBs at higher energies or from vantage points outside the ecliptic plane could provide crucial data for a complete understanding of their accurate spatial distribution.
3. *Progenitor Clues Despite Biases.* The identified subclusters within the GRB population using the mixture model might still hold valuable clues about progenitor environments. By carefully considering and potentially correcting for observational biases, future investigations can explore correlations between these clusters and other GRB properties, revealing insights into the stellar or binary system configurations that lead to GRB formation.

7. Further Discussion

1. The analysis delves into pertinent parameters' probabilistic circular distributional properties. Given the directional nature of specific parameters, particularly concerning the Galactic coordinates of observed GRBs, circular statistical methodologies were employed. Notably, circular distributions were scrutinized, and a von Mises Fisher mixture spherical distribution with an optimal number of 2 mixtures was fitted for the Whole BATSE catalog. Similarly, two mixtures of von Mises Fishers were identified for Long and Short GRBs (see Tables 1, 3, and 5).

Table 11
Table Containing the Bayesian Information Criteria Score for Each K Value

Partition Number	BIC Values	Partition Number	BIC Values
1	−943.9735	6	−1002.5893
2	−1039.3358	7	−989.8878
3	−1031.3133	8	−971.9138
4	**−1041.3955**	9	−954.0112
5	−1016.1941	10	−936.1367

Note. From that, 4 partitions can combine Fisher Von Mises Distribution for Short Fermi Gamma-Ray Bursts' location parameters (GLON and GLAT). We checked ten values of k from 1 to 10, where the optimal number of partitions is 4.

Table 12
Table Showing the BC Values Divided by 595

Partition Number	BC values	Partition Number	BC values
1	−1268.85	6	−123955.49
2	−6708.19	7	−51428.21
3	−4624.12	8	−36605.81
4	−11578.99	9	−51829.63
5	**−132521.47**	10	−52391.59

Note. The optimal number of partitions is 5.

2. Additionally, an investigation was conducted to ascertain whether the location parameter of BATSE GRBs follows any spherical distribution (refer to Table A1).
3. Likewise, a similar approach was employed for FERMI GRBs, particularly concerning the Galactic coordinates of observed GRBs. Circular distributions were analyzed, and a von Mises Fisher mixture spherical distribution with an optimal number of 3 mixtures was fitted for the Whole FERMI catalog. Similarly, four mixtures of von Mises Fishers were identified for Long and Short GRBs (refer to Table A4).
4. Analogously, an assessment was conducted to determine if the location parameter of FERMI GRBs conforms to any spherical distribution (see Table A4).
5. The classification into short-hard and long-soft GRBs is primarily based on the bimodal distribution of burst durations ($T50$, $T90$) and is further supported by the hardness ratio, which distinguishes bursts with harder spectra (short GRBs) from those with softer spectra (long GRBs).
6. Our position within the Milky Way could introduce a heliocentric bias, favoring the detection of GRBs in certain sky regions over others. Although BATSE and Fermi-GBM have overlapping sky coverage, the observer's location may still influence the observed distribution. Future studies should consider modeling the observer's position relative to the Galactic plane to mitigate this bias.

In conclusion, our findings suggest a non-isotropic distribution for GRBs, even with limitations from the Milky Way and our observing position. Further efforts to mitigate these biases and data from future missions are crucial to solidify this conclusion. Nevertheless, if confirmed, the observed non-isotropy offers exciting possibilities for understanding the Universe's large-scale structure, refining GRB rate estimates, and uncovering clues about the environments that give rise to these powerful explosions.

8. Conclusion

Our investigation into the spatial distribution of GRBs using directional statistical methodologies has revealed compelling evidence for a non-isotropic distribution of these extraordinary cosmic events. Through rigorous statistical analyses of both the BATSE and Fermi GRB catalogs, we have demonstrated that the assumption of isotropy, which has underpinned numerous theoretical models, may not fully capture the true nature of GRB distribution.

8.1. Key Findings

The Watson test results, coupled with the optimal partitioning identified by the BIC and BC, strongly suggest that GRBs are not uniformly distributed across the sky. Our analysis indicates that BATSE and Fermi GRBs exhibit significant clustering patterns deviating from isotropy.

By employing vMF mixture models, we have characterized the spatial distribution of GRBs in terms of GLON and GLAT. The optimal number of mixture components varied between data sets but consistently pointed towards multiple components, reinforcing the presence of underlying structure in GRB spatial distribution. Applying directional statistical techniques has allowed us to identify distinct sub-clusters within the GRB population. These clusters potentially correlate with different progenitor environments or mechanisms, providing a new dimension to the study of GRB origins. The detailed tables about the watson test and AIC are given in the tables below from Table A1–A12.

8.2. Implications

Even under certain limitations and assumptions, the discovery of a non-isotropic distribution of GRBs could have profound implications for our understanding of their origins and the universe's large-scale structure. The observed clustering may reflect regions of enhanced star formation or specific

types of galaxies, suggesting that GRBs can serve as tracers of the large-scale structure of the cosmos. Revising the assumption of isotropy in GRB distribution can lead to more accurate estimates of their occurrence rate, providing deeper insights into the frequency and conditions of these powerful events. Additionally, the distinct clusters identified through our analysis offer new avenues for exploring the environmental and physical conditions that lead to different types of GRBs, enhancing our understanding of the progenitor systems and the processes driving these cosmic explosions.

8.3. Criticism

The von Mises and Von Mises Fisher Fisher distribution comes from a maximizing Shannon entropy under first and second-moment restriction; see Jammalamadaka & SenGupta (2001), Ghosh et al. (2024a). Although ideally, we regard this maximum entropic assumption as a strong point of this paper, the door for potential criticism is open. The observed anisotropy in the spatial distribution of GRBs raises intriguing questions about the underlying causes of this non-uniformity. One potential factor could be the inherent limitations of using 2D image data sets, which project the celestial sphere onto a flat surface, potentially introducing distortions and biases. This projection can obscure the true 3D spatial relationships between GRBs, leading to artificial clustering patterns that may only partially reflect their distribution in three-dimensional space. Additionally, the assumption of isotropy may hold more validity in a truly 3D context, where the full extent of the universe's structure and the distribution of matter can be more accurately represented. 2D data might fail to capture complex spatial relationships, such as those influenced by the universe's large-scale structure, gravitational lensing, or other cosmological phenomena. Therefore, while our findings suggest anisotropy, they must be interpreted cautiously, acknowledging the potential artifacts introduced by the 2D nature of the data sets. Future studies employing 3D data and advanced modeling techniques will be crucial to validate these findings and provide a more comprehensive understanding of GRB distribution in the cosmos.

One significant limitation of our analysis stems from the potential bias introduced by Milky Way obscuration. Regions near the Galactic plane are underrepresented in the data set due to the effects of dust and gas, which obscure observations and potentially impact the accuracy of our directional analysis. While this issue has been addressed in the revised Discussion and Criticism sections, it remains a critical limitation of the current work.

To mitigate this bias in future analyses, detailed modeling of the dust and gas distributions within the Milky Way will be necessary. Such modeling would enable more accurate corrections for obscured regions, ensuring a more balanced representation of the entire sky. By incorporating these corrections, future studies could provide a clearer and more comprehensive understanding of the phenomena being investigated.

Nonetheless, our study statistically inquires about the long-held assumption of isotropy in GRB distribution and paves the way for a deeper understanding of these enigmatic explosions. By leveraging advanced statistical techniques and future observational data, we can unlock new insights into the cosmos's most luminous events and their role in the universe's grand tapestry.

9. Future Work

In our exploration of the spatial distribution of GRBs using directional statistical methods, several promising avenues for future work emerge:

1. Refine classification based on Latent variable models: Future investigations could delve into more sophisticated models, including, but not limited to, latent variable models, and could potentially provide even more nuanced classifications of GRBs based on their directional properties.
2. Investigate physical correlations: The proposed future classification based on spherical mixture distributions has the potential to serve as a powerful tool for further exploration. Researchers may uncover crucial insights into the physical processes governing these enigmatic explosions by correlating the identified classes with physical parameters of GRBs, such as redshift, energy fluence, or associated host galaxies. For example, a specific cluster might be related to GRBs originating in a particular environment or having a distinct progenitor star.
3. Multi-messenger analysis: The field of multi-messenger astronomy is rapidly evolving, and future studies could integrate data from other astronomical messengers, such as gravitational waves or neutrino detections, alongside the established GRB catalogs. This broader approach could offer a more holistic perspective on GRBs' spatial distribution and physical properties within the grand tapestry of the Universe. By combining information from different wavelengths and messengers, scientists may be able to elucidate the complete picture of GRB formation and their role in the Universe's evolution.
4. *Mitigating Possible Heliocentric Bias and Correcting for Possible Milky Way Obscuration.* Future efforts must address Milky Way obscuration through dust maps and multi-wavelength observations while mitigating heliocentric bias with next-generation all-sky surveys and advanced statistical modeling. Refining the mixture model to account for these biases and correlating subclusters with host galaxy properties will further solidify our understanding of GRB distribution. This will lead to

more accurate large-scale structure maps, improved rate estimates, and a clearer picture of GRB progenitor environments. Both BATSE and Fermi-GBM data are known to have significant localization uncertainties, which inherently influence the precision of our directional analysis. To address these uncertainties, we employed von Mises-type variability factors, which are well-suited for spherical geometries. These factors were incorporated into the model to treat GRB positions as random variables, with location points modeled to account for von Mises-type variability. However, handling "notorious outliers" remains a critical aspect that our current model does not explicitly address. While the model is flexible in managing overall uncertainties, it does not include specific mechanisms to detect and handle outliers that might disproportionately influence parameter estimates or misrepresent underlying patterns. Future work will focus on developing and incorporating robust outlier detection and mitigation techniques to ensure the reliability of results in the presence of such data anomalies. This enhancement would not only strengthen the robustness of our analysis but also broaden the applicability of the model to data sets with complex variability and potential outliers.

5. In Chapter 3 and Chapter 2 of Wang et al. (2022), they discussed the topic of isotropic (Euclidean and Spherical domain), where they were able to create a suitable basis using Bernstein polynomials. They provide sufficient conditions for equivalence and orthogonality of Gaussian measures on spheres with isotropic covariance functions depending on the great circle distance and illustrate the asymptotic property of parameter estimation for a list of parametric covariance families. Which can be used in the future for the spatial analysis of GRB locations.
6. Future analyses could improve the accuracy of short GRB isotropy assessments by excluding known soft gamma repeaters (SGRs), which are typically very short-duration bursts (0.1 s) and may originate from Galactic sources, thereby potentially biasing the isotropy results.
7. While Swift-BAT provides more precise localizations compared to BATSE and Fermi-GBM, the focus of this study was to analyze the older BATSE and Fermi catalogs to assess potential anisotropies across different observational eras. Incorporating Swift-BAT data could be a valuable extension of this work to evaluate whether improved localization affects the observed distribution patterns.
8. Future efforts requires to address Milky Way obscuration through dust maps and multi-wavelength observations while mitigating heliocentric bias with next-generation all-sky surveys and advanced statistical modeling. Refining the mixture model to account for these biases and correlating sub-clusters with host galaxy properties will further solidify our understanding of GRB distribution. This will lead to more accurate large-scale structure maps, improved rate estimates, and a clearer picture of GRB progenitor environments.

Code Availability

The code about GRB and the data sets can be found at the following link: https://github.com/Prithwish-ghosh/GRB_CIRCULAR.

Competing Interests

No Competing Interests

Data Availability

The data used for this article can be accessed through the links provided below.

1. The first data set, which contains information about the BATSE GRB, can be found at the following link: https://ui.adsabs.harvard.edu/link_gateway/1999ApJS..122..465P/CDS.
2. The second data set provides valuable FERMI GRB information and is available at https://ui.adsabs.harvard.edu/link_gateway/2020ApJ...893...46V/CDS.

Funding Statement

No Funding available.

Appendix
Directional Statistics Preliminaries and Additional Results

A.1. Von Mises Distribution

The Von Mises distribution is a probability distribution commonly used to model circular data, such as directions around a circle (e.g., compass angles, wind directions) (Jammalamadaka & SenGupta 2001). Under moment constraints, the Von Mises distribution maximizes entropy compared to other probability distributions capable of representing circular data (Mardia et al. 2000; Jammalamadaka & SenGupta 2001). Given the specified constraints, it reflects the state of maximum disorder. It allows for characterizing the distribution of observations with a preferred direction and a certain level of dispersion around that direction (Ghosh et al. 2024a, 2024b).

A circular random variable θ follows the Von Mises distribution (also known as the Circular Normal Distribution and a close approximation to the wrapped normal distribution)

Table A1
Watson Test Results are Given Here, Where We used Both 0.01 Significance Levels

Parameter	Test Statistics	Critical Value	Distribution
GLON	0.0329	0.081	von Mises
GLAT	0.0842	0.081	Not von Mises

Note. We tested if the directional parameters (GLON, GLAT) GRB observed data points and checked whether they follow any circular distributions. According to the results above, all the location parameters of GRB follow the von Mises distribution. and circular distributions.

Table A2
Watson Test Results are Given Here, Where we used Both 0.01 Significance Levels

Parameter	Test Statistics	Critical Value	Distribution
GLON	0.0329	0.081	von Mises
GLAT	0.0901	0.081	Not von Mises

Note. We tested if the directional parameters (GLON, GLAT) for Long GRB observed data points and checked whether they follow circular distributions. According to the results above, all the location parameters of GRB follow the von Mises distribution. and circular distributions.

Table A3
Watson Test Results are Given Here, Where We used Both 0.01 Significance Levels

Parameter	Test Statistics	Critical Value	Distribution
GLON	0.0221	0.081	von Mises
GLAT	0.027	0.081	von Mises

Note. We tested if the directional parameters (GLON, GLAT) for Short GRB observed data points and checked whether they follow circular distributions. According to the results above, all the location parameters of Short GRB follow the von Mises distribution. and circular distributions.

Table A4
Watson Test Results are Given Here, Where We used Both 0.01 Significance Levels

Parameter	Test Statistics	Critical Value	Distribution
GLON	0.0585	0.081	von Mises
GLAT	0.0234	0.081	von Mises

Note. We tested whether the directional parameters (GLON, GLAT) for Fermi GRB observed data points and checked whether they follow circular distributions. According to the results above, all the location parameters of Fermi GRB follow the von Mises distribution. and circular distributions.

and is characterized by the probability density function (pdf):

$$f(\theta;\, \mu,\, k) = \frac{1}{2\pi I_0(k)} e^{k\cos(\theta-\mu)}, \tag{A1}$$

where θ lies in the range $[0, 2\pi)$, μ is constrained to $[0, 2\pi)$, and $k > 0$. The normalizing constant $I_0(k)$ is the modified Bessel function of the first kind and order zero.

Table A5
Watson Test Results are Given Here, Where We used Both 0.01 Significance Levels

Parameter	Test Statistics	Critical Value	Distribution
GLON	0.0332	0.081	von Mises
GLAT	0.0222	0.081	von Mises

Note. We tested whether the directional parameters(GLON, GLAT) for Long Fermi GRB observed data points and checked whether they follow circular distributions. According to the results above, all the location parameters of Long Fermi GRB follow the von Mises distribution. and circular distributions.

Table A6
Watson Test Results are Given Here, Where We used Both 0.01 Significance Levels

Parameter	Test Statistics	Critical Value	Distribution
GLON	0.0579	0.081	von Mises
GLAT	0.0137	0.081	von Mises

Note. We tested whether the directional parameters (GLON, GLAT) for Short Fermi GRB observed data points and checked whether they follow circular distributions. According to the results above, all the location parameters of Short Fermi GRB follow the von Mises distribution. and circular distributions.

Table A7
AIC Values for Number of Mixture Components $k = 1, 2, \ldots$. From that, 6 Partitions can Combine Fisher Von Mises Distribution for the Location Parameter (GLON and GLAT)

Partition Number	AIC Values	Partition Number	AIC Values
1	−5377.084	**6**	**−5968.205**
2	−5929.94	7	−5964.475
3	−5941.008	8	−5958.653
4	−5947.523	9	−5944.605
5	−5950.162	10	−5946.341

Note. We checked ten values of k from 1 to 10, where the optimal number of partitions is 6.

Table A8
Table Containing the AIC for Each K Value

Partition Number	AIC Values	Partition Number	AIC Values
1	−3562.885	**6**	**−3925.29**
2	−3903.533	7	−3909.163
3	−3910.43	8	−3920.66
4	−3910.581	9	−3900.531
5	−3910.182	10	−3913.492

Note. From that, 6 partitions can combine Fisher von Mises Distribution for Long Gamma-Ray Bursts' location parameters (GLON and GLAT). We checked ten values of k from 1 to 10, where the optimal number of partitions is 6.

Table A9
This Table Contains the AIC for Each K Value

Partition Number	AIC Values	Partition Number	AIC Values
1	−1810.712	6	−2020.543
2	**−2019.927**	7	−2014.905
3	−2019.444	8	−2009.226
4	−2019.891	9	−2003.559
5	−2019.828	10	−1997.461

Note. From that, 2 partitions can combine Fisher Von Mises Distribution for Long Gamma-Ray Bursts' location parameters (GLON and GLAT). We checked ten values of k from 1 to 10, where the optimal number of partitions is 2.

Table A10
Table Containing the AIC for Each K Value

Partition Number	AIC Values	Partition Number	AIC Values
1	−5878.347	6	−6536.534
2	−6493.639	7	−6535.145
3	−6536.187	8	−6536.654
4	−6542.456	9	−6534.008
5	**−6543.828**	10	−6533.199

Note. From that, 5 partitions can combine Fisher Von Mises Distribution for the location parameter (GLON and GLAT) of Fermi Gamma-Ray Bursts. We checked ten values of k from 1 to 10, where the optimal number of partitions is 5.

Table A11
Table Containing the AIC Score for Each K Value

Partition Number	AIC Values	Partition Number	AIC Values
1	−4927.579	6	−5459.467
2	−5433.957	7	−5432.773
3	−5461.554	8	−5457.136
4	**−5461.783**	9	−5458.516
5	−5474.766	10	−5460.938

Note. From that, 4 partitions can combine Fisher Von Mises Distribution for Long Fermi Gamma-Ray Bursts' location parameters (GLON and GLAT). We checked ten values of k from 1 to 10, where the optimal number of partitions is 4.

Table A12
Table Containing the AIC for Each K Value

Partition Number	AIC Values	Partition Number	AIC Values
1	−951.9313	6	−1066.704
2	−1059.23	7	−1069.36
3	−1073.228	8	−1058.28
4	**−1075.128**	9	−1057.449
5	−1071.109	10	−1051.437

Note. From that, 4 partitions can combine Fisher Von Mises Distribution for Short Fermi Gamma-Ray Bursts' location parameters (GLON and GLAT). We checked ten values of k from 1 to 10, where the optimal number of partitions is 4.

To determine the cumulative distribution function (cdf) of the Von Mises distribution, we integrate the pdf, resulting in:

$$F(\theta) = \frac{1}{2\pi I_0(k)}\left(\theta I_0(k) + 2\sum_{p=1}^{\infty}\frac{I_p(k)\sin p(\theta-\mu)}{p}\right), \quad \text{(A2)}$$

where θ is confined to the interval $[0, 2\pi)$.

A.2. Watson Test

In this study, Watson (1982), we primarily employ Watson-type tests to examine whether the positional data adhere to either a Von Mises Distribution or a Circular Uniform Distribution (Ghosh et al. 2024b):

$$W_n^2 = \int_0^{2\pi}\left[(F_n - F) - \int_0^{2\pi}(F_n - F)\,dF\right]^2 dF, \quad \text{(A3)}$$

where W_n represents Watson's statistic, $F_n(\alpha)$ denotes the empirical distribution function, and $F(\alpha)$ represents the actual distribution function. Critical values for Watson's U^2 test at $\alpha = 0.01$ were obtained from standard statistical tables (see Mardia et al. 2000; Jammalamadaka & SenGupta 2001) and implemented using the "circstats" package in R. This ensures that the test maintains the desired significance level when evaluating the null hypothesis of uniformity on the celestial sphere.

All the detailed analysis of the above mentioned tests and all are given in the Tables A1–A12.

ORCID iDs

Prithwish Ghosh https://orcid.org/0000-0001-7747-5045
Sujit Ghosh https://orcid.org/0000-0001-8351-408X
Debashis Chatterjee https://orcid.org/0000-0002-0991-7574

References

Aasi, J., Abbott, B., Abbott, R., et al. 2014, PhRvD, 89, 122004
Abbott, B. P., Abbott, R., Abbott, T. D., et al. 2017a, ApJ, 841, 89
Abbott, B. P., Abbott, R., Abbott, T. D., et al. 2017b, ApJL, 848, L13
Ajello, M., Baldini, L., Ballet, J., et al. 2021, ApJ, 921, 144
Akerlof, C. W., & Swan, H. F. 2007, ApJ, 671, 1868

Anchordoqui, L. A., Mechmann, C., & Soriano, J. F. 2020, JHEAp, 25, 23
Andrade, U., Bengaly, C. A. P., Alcaniz, J. S., & Capozziello, S. 2019, MNRAS, 490, 4481
Bagoly, Z., Mészáros, A., Horváth, I., Balázs, L. G., & Mészáros, P. 1998, ApJ, 498, 342
Balastegui, A., Ruiz-Lapuente, P., & Canal, R. 2001, MNRAS, 328, 283
Baumgart, C. W. 1994, Proc. SPIE, 2243, 552
Bhat, P. N., Meegan, C. A., von Kienlin, A., et al. 2016, ApJS, 223, 28
Bloom, J. S., Prochaska, J., Pooley, D., et al. 2006, ApJ, 638, 354
Boch, T., Oberto, A., Fernique, P., & Bonnarel, F. 2011, in ASP Conf. Ser. 442, Astronomical Data Analysis Software and Systems XX, ed. I. N. Evans et al. (San Francisco, CA: ASP), 683
Calderone, G., Ghirlanda, G., Ghisellini, G., et al. 2015, MNRAS, 448, 403
Charisi, M., Márka, S., Bartos, I., et al. 2015, MNRAS, 448, 2624
Chatterjee, D., & Ghosh, P. 2023, Available at SSRN 4822664
Chatterjee, D., & Ghosh, P. 2024, PASP, 136, 114509
Chattopadhyay, T., Misra, R., Chattopadhyay, A. K., & Naskar, M. 2007, ApJ, 667, 1017
Chen, J. 1995, Optimal Rate of Convergence for Finite Mixture Models, AnStat, 23, 221
Connaughton, V., Briggs, M. S., Goldstein, A., et al. 2015, ApJS, 216, 32
Dezalay, J. P., Barat, C., Talon, R., et al. 1992, Short Cosmic Events: A Subset of Classical GRBs?, American Institute of Physics Conference Series in AIP Conf. Ser. 265 *(Melville, NY, Jan 1992)* ed. W. S. Paciesas & G. J. Fishman (Melville, NY: AIP), 304
Ding, J., Tarokh, V., & Yang, Y. 2017, ITIT, 64, 4024
Duque, J. C., & Marinucci, D. 2023, AnRSA, 11
Fishman, G. J., & Meegan, C. A. 1995, ARA&A, 33, 415
Fleischer, C. 2012, Can Sequentially Linked Gamma-Ray Bursts Nullify Randomness?, arXiv:1205.0518
Fynbo, J. P., Watson, D., Thöne, C. C., et al. 2006, Natur, 444, 1047
García-Portugués, E. 2013, EJSta
Gehrels, N., Fichtel, C. E., Fishman, G. J., Kurfess, J. D., & Schönfelder, V. 1993, SciAm, 269, 68
Gehrels, N., Norris, J., Barthelmy, S., et al. 2006, Natur, 444, 1044
Gehrels, N., Sarazin, C., O'brien, P., et al. 2005, Natur, 437, 851
Ghosh, P., & Chakraborty, S. 2022, in Proc. 16th Int. Conf. MSAST, 21, Online
Ghosh, P., & Chatterjee, D. 2023, A Novel Spherical Statistics-based Spatio-Temporal Analysis to Unveil Distributional Properties of Meteor Strike on Earth, (unpublished doctoral dissertation, Visva Bharati
Ghosh, P., Chatterjee, D., & Banerjee, A. 2024a, MNRAS, 531, 1294
Ghosh, P., Chatterjee, D., Banerjee, A., & Das, S. S. 2024b, PLoSO, 19, e0304279
Goldstein, A., Burgess, J. M., Preece, R. D., et al. 2012, ApJS, 199, 19
Goldstein, A., Fletcher, C., Veres, P., et al. 2020, ApJ, 895, 40
Gruber, D., Goldstein, A., von Ahlefeld, V. W., et al. 2014, ApJS, 211, 12
Hakkila, J., Giblin, T. W., Roiger, R. J., et al. 2003, ApJ, 582, 320
Hakkila, J., Haglin, D. J., Pendleton, G. N., et al. 2000a, ApJ, 538, 165
Hakkila, J., Haglin, D. J., Roiger, R. J., et al. 2000b, in AIP Conf. Proc. 526 (Melville, NY: AIP), 33
Hakkila, J., Meegan, C. A., Pendleton, G. N., et al. 1994, AJ, 422, 659
Ho, N., & Nguyen, X. 2016, EJSta, 10, 271
Horváth, I. 1998, ApJ, 508, 757
Horváth, I., Balázs, L. G., Bagoly, Z., Ryde, F., & Mészáros, A. 2006, A&A, 447, 23
Jammalamadaka, S. R., & SenGupta, A. 2001, Topics in Circular Statistics, Vol. 5 (Singapore: World Scientific)
Kaneko, Y., Bostanci, Z. F., Göğüş, E., & Lin, L. 2015, MNRAS, 452, 824
Kim, S., & SenGupta, A. 2018, in Statistics and its Applications: Platinum Jubilee Conf., Kolkata, India, December 2016, (Berlin: Springer), 25
King, A., Olsson, E., & Davies, M. B. 2007, MNRAS: Letters, 374, L34
Koshut, T. M., Paciesas, W. S., Kouveliotou, C., et al. 1996, ApJ, 463, 570
Kouveliotou, C., Meegan, C. A., Fishman, G. J., et al. 1993, ApJL, 413, L101
Kovacevic, M., Izzo, L., Wang, Y., et al. 2014, A&A, 569, A108
Levan, A. J., Gompertz, B. P., Salafia, O. S., et al. 2024, Natur, 626, 737
Mardia, K. V. 1972, Statistics of Directional Data Academic) (New York:
Mardia, K. V., Jupp, P. E., & Mardia, K. 2000, Directional Statistics, Vol. 2 (Wiley Online Library)
McLean, B. J., Golombek, D. A., Hayes, J. J., & Payne, H. E. 2012, in New Horizons from Multi-Wavelength Sky Surveys: Proc. 179th Symp. Int. Astronomical Union, Held in Baltimore, August 26-30, 1996, Vol. 179 (USA: Springer Science & Business Media)
Meegan, C., Fishman, G., Wilson, R., et al. 1992, Natur, 355, 143
Mukherjee, S., Feigelson, E. D., Babu, G. J., et al. 1998, ApJ, 508, 314
Paciesas, W. S., Meegan, C. A., Pendleton, G. N., et al. 1999, ApJS, 122, 465
Piran, T. 1992, ApJL, 389, L45
Piran, T. 2005, RvMP, 76, 1143
Preece, R. D., Briggs, M. S., Mallozzi, R. S., et al. 2000, ApJS, 126, 19
Rastinejad, J. C., Gompertz, B. P., Levan, A. J., et al. 2022, Natur, 612, 223
Sazonov, S. Y., Lutovinov, A., & Sunyaev, R. 2004, Natur, 430, 646
Schaefer, B. E., & Xiao, L. 2006, arXiv:astro-ph/0608441
Soderberg, A., Kulkarni, S., Berger, E., et al. 2004, Natur, 430, 648
Svinkin, D., Aptekar, R., Golenetskii, S., et al. 2019, J. Phys.: Conf. Ser., 1400, 022010
Tarnopolski, M. 2015, A&A, 581, A29
von Kienlin, A., Gruber, D., Kouveliotou, C., et al. 2012, ApJ, 755, 150
von Kienlin, A., Meegan, C. A., Paciesas, W. S., et al. 2014, ApJS, 211, 13
Von Kienlin, A., Meegan, C., Paciesas, W., et al. 2020, ApJ, 893, 46
Wang, Y., et al. 2022, Covariance Function Estimation and Causal Inference Methods, North Carolina State University
Watson, G. S. 1982, Journal of Applied Probability, 19, 265
Woosley, S., & Bloom, J. 2006, ARA&A, 44, 507
Yu, H.-F., Preece, R. D., Greiner, J., et al. 2016, A&A, 588, A135
Zhang, J., Yang, Y., & Ding, J. 2023, Wiley Interdisciplinary Reviews: Computational Statistics, 15, e1607